scientific reports

Check for updates

OPEN

Design and experiment of a comb-and-scrape Idesia Polycarpa Maxim threshing device

Guoqiang Yang[1], Di Wu[1]✉, Weiping Xu[1] & Yong Tang[2]

Currently, Idesia polycarpa Maxim is used as a woody oil crop and the edible oil extracted from it has a very high unsaturated fatty acid content. Therefore, this crop has also been increasingly planted industrially. However, its fruit picking work relies on manual use of high pruning shears to complete, the efficiency is low. Based on this problem, this paper designs an integrated device for picking and threshing. After the relevant physical properties of the fruit were tested, the harvesting method was indeed brush-type harvesting. Then the test was carried out by simulation using comb plates with different cross-sectional shapes. The results show that the maximum separating force on a single grain produced by a comb plate with a diamond-shaped cross-section is 15 N, which is larger than that produced by a rectangular shape (7.5 N) and a circular shape (2.1 N), and the vibrational agitation produced by the fruit is minimized under the operation of a diamond-shaped comb plate. The experiments with cross-section shape as a single factor also showed that the diamond-shaped cross-section shape comb plate has more excellent threshing effect. On this basis, the performance indexes of picking rate, breakage rate and stalking rate, the factors of comb gap and comb moving speed were used to conduct the bench test, and the response surface analysis of the central combination design was carried out. The results showed that the three performance indexes were best when the comb gap was 4.4 mm and the traveling speed was 0.06 m/s. Validation experiments were conducted using this optimal parameter combination, and the results showed that the picking clean rate, breakage rate, and rate with stalks were increased by 8.01%, 34.33%, and 5.41%, respectively, compared with those before optimization. The design of this device can solve the problem of mechanized picking of santolina and provide design ideas for the picking of cluster-shaped granular crops.

Keywords Idesia Polycarpa Maxim, Threshing and harvesting, Simulation and emulation, Response surface analysis

Idesia polycarpa Maxim, belonging to the family Daphniaceae (formerly Flacourtiaceae), is a deciduous tree species of the genus Idesia[1,2]. These trees typically reach heights of 8–21 m, though cultivated varieties are often maintained at 3–4 m through dwarfing techniques. The Idesia polycarpa Maxim is particularly valuable due to its high content of linoleic acid and linolenic acid[3–5], which have demonstrated beneficial effects on human blood lipids and thrombosis prevention[6,7].

The growth environment of the Idesia polycarpa Maxim is mostly on high-altitude slopes,

valleys, and deciduous broad-leaved forests and mixed coniferous-broad-leaved forests. Moreover, due to the high position of the Idesia polycarpa Maxim, it brings great difficulties to the harvest. The harvest period often requires a lot of manual labor to rely on ladders, high-branch shears, and other tools for harvesting. As the economic cost of harvesting increases, it is often missed the best harvest time due to low harvest efficiency[8–10]. This will directly affect the quality of the Idesia polycarpa Maxim itself and the products processed at the next level. Therefore, some Idesia polycarpa Maxim are difficult to harvest, causing waste of resources.

However, the research on the Idesia polycarpa Maxim at home and abroad mainly focuses on the improvement of oil extraction methods and the optimization of related chemical component extraction technologies[11–13]. In addition to this, there are also sections dedicated to biology[14–16] and medicine[17–19]. However, there are deficiencies in the methods and means of mechanized harvesting. For crops with special cluster shape and fruit shape, the existing picking methods include comb type, shear type and vibrating type. Existing studies include a negative pressure rotary cutting harvesting device for safflower silk designed by Chen Bangbang et al. which has

[1]College of Mechanical and Electrical Engineering, Guizhou Normal University, Guiyang 550025, Guizhou, China. [2]Agricultural Machinery Technology Extension Station, Guiyang 550003, Guizhou, China. ✉email: munichlife@163.com

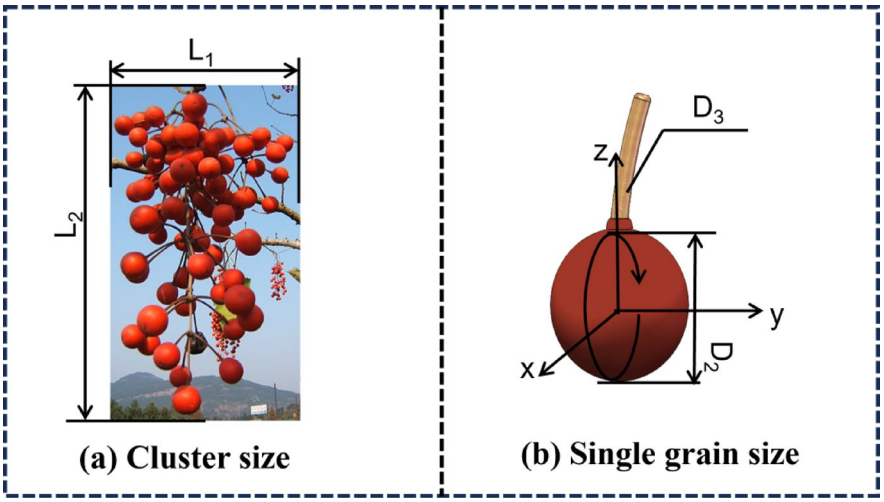

Fig. 1. Cluster and grain size parameters.

Parameters	Average value	Standard deviation	Variation coefficient
Particle size /(mm)	7.36	0.20	2.72
Fruit stem diameter/(mm)	0.60	0.036	6.00
Height of entire cluster/(mm)	15.12	1.43	9.46
Weight of berries /(g)	0.25	0.14	56
Whole cluster diameter/(mm)	12.67	0.42	3.32

Table 1. Berry whole cluster and single grain parameters.

the characteristics of small size and suitable for mountain use[20]. The Yunnan edible rose pruner designed by Zhu Huibin et al., has a comb-like end effector that effectively prevents damage to the inflorescence[21]. Li Tianyu et al. designed a shear harvesting device for fresh corn, which has the characteristics of low power consumption and low damage[22]. Ghonimy et al. used the principle of vibration to explore olives[23]. Liu Changyi et al. used vibration to harvest walnuts[24], and Wucheng et al. used vibration devices to harvest Camellia oleifera fruits[25]. The above different harvesting methods have great reference value for one type of crop. However, the berries are further processed after harvesting, and the stems cannot be processed at the same time. Threshing is still required after harvesting with a shear unit. Therefore, in view of this characteristic, a comb type device was selected to be designed to harvest it.

For the comb-type picking device. Chen Haixia developed a combing stick structure incorporating flexible rubber wires and elastic teeth for alfalfa seed harvesting, utilizing leverage principles for seed casting and collection[26]. However, this design proves less suitable for Idesia polycarpa due to insufficient lightness and potential interference with fruit-bearing branches. Xu Fulong et al. designed a test bench featuring an eccentric swing mechanism and combing device for flax and sesame[27]. while Fang Dawei et al. created a comb-tooth fruit picking test bench. Both designs are limited to terrestrial, upward-growing cluster crops and are unsuitable for suspended-growth species[28]. Wang Hongxuan et al. designed a differential comb type pineapple harvester[29], the comb type of working part of the space required is larger, and Idesia Polycarpa Maxim not only the fruit position of the hanging is high and the working space is limited. Thus, it is not applicable. In addition, there are comb-type devices for picking granular crops and flowery crops[30–34]. In summary, this paper has designed a mechanized harvesting device for the integrated picking and threshing of Idesia Polycarpa Maxim.

Materials and methods

Physical properties of the Idesia Polycarpa Maxim.

Harvested mature Idesia Polycarpa Maxim for measurement. Obtaining whole tree and single seed size parameters and their basic appearance is shown in Fig. 1.after measurement, the height of the whole cluster of plants L_1 ranges from 10 mm to 12 mm, and the diameter of the whole cluster L_2 ranges from 130 mm to 200 mm. As shown in Fig. 1a. The granule size of Idesia Polycarpa Maxim seeds D_2 ranges from 6 mm ~ 10 mm, and its stalk D_3 ranges from 0.6 mm ~ 1.4 mm. As shown in Fig. 1b. Sixty seeds were randomly picked at maturity and the mean, standard deviation and coefficient of variation were calculated after the determination of the dimensional parameters and the results are shown in Table 1.

After sorting out the particle size of the randomly picked mountain tree. The Origin software was used to calculate the mean value, standard deviation and other parameters of particle size. Then select the normality test

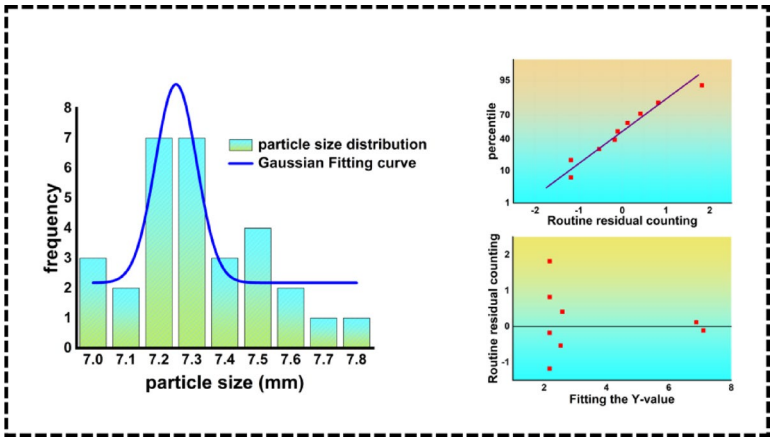

Fig. 2. Particle size distribution and Gaussian function fitting curve.

Name	average value	standard deviation	Variation coefficient
Small size fruit-stalk binding	4.50	0.59	13.11
Big size fruit-stalk binding	6.55	0.66	10.07
Fruit stalk-stem binding in small sizes	7.98	0.63	7.89
Fruit stalk-stem binding in big sizes	21.4	4.33	20.23

Table 2. Binding force test parameters. Note: Small fruits are berries with a grain size of less than 8.5 mm, large fruits are berries with a grain size including 8.5 mm or more.

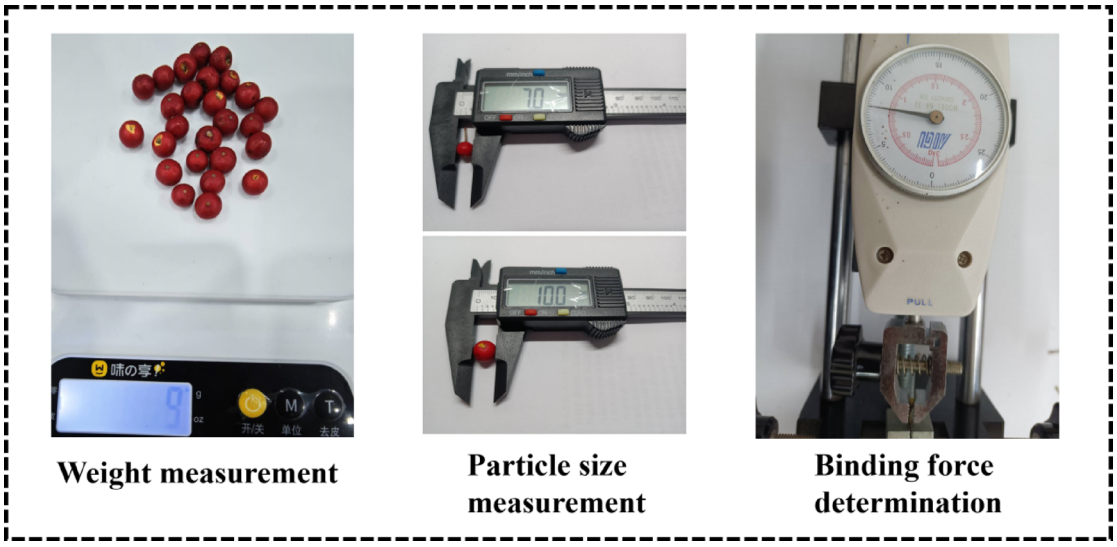

Fig. 3. Physical parameter measurement experiment.

in the statistical options. The results show that at the level of 0.05, the data significantly conform to the normal distribution, so the Gaussian function is used to fit it, and the distribution plot is obtained as shown in Fig. 2.

To ensure the fruit detaches smoothly, the sum of the external forces applied must be greater than the fruit-stem adhesion force itself. Therefore, the AIGU Aiguo horizontal pointer-type push-pull force gauge (model: NK-30; range: 30 N) was used for the test, and the measured data is shown in Table 2. All the above physical parameter measurement experiments are shown in Fig. 3.

Derivation of shedding force of Idesia Polycarpa Maxim

The expected picking effect is that a large number of berries and stems achieve separation. However, during the picking process, due to the flexibility of his peduncle and the lower berries, they have a certain degree of

viscoelasticity[35]. Therefore, in the derivation, for the convenience of calculation, it is considered as a stationary plant. When the equipment enters the threshing working state, the device maintains a vertical relationship with the axis of the whole cluster of Idesia Polycarpa Maxim. In the process of continuously increasing the downward pressure, the berries and stems begin to separate continuously. Therefore, it can be fully considered that under the combined action of the holding force provided at the main stem and the self-binding force of the fruit, the threshing work can be completed smoothly. The relevant parameters need to be analyzed by mechanics, and the force analysis is shown in Fig. 4.

When the combing and scraping action is started by the combing mechanism, it can be obtained from the overall force:

$$F_j + F_s \geq (G + F_c + 2F_y) \cdot n \tag{1}$$

Where F_j is the main stalk of the plant and the upper branch of the fruit tree itself (N). F_s is the friction force provided by the main stalk of the plant after clamping the serrated clamping plate (N). G is the gravity force (N) of the plant itself under the standard gravitational acceleration (9.8 m/s^2). F_c is the main extrusion force provided by the comb plate in the vertical direction (N). $2F_y$ is the force synthesized by the force diagonally below the two ends (N). n is a certain creep in consideration of the force process, in order to improve the safety of the entire calculation process. Special provisions for substitution into the calculation of the safety coefficient, take $n = 1.2$.

Among them:

$$F_s = F_N \cdot \mu \tag{2}$$

where μ is the friction coefficient between wood and rubber, and μ is 0.45;

From the force distribution relationship in Fig:

$$F_y = F \cdot sin\alpha = F \cdot \frac{S}{\sqrt{S^2 + \left(\frac{d}{2}\right)^2}} \tag{3}$$

Substituting Eqs. (2) and (3) into Eq. (1) yields:

$$F_N \geq \frac{\left[G + F_c + \frac{2 \cdot F \cdot S}{\sqrt{S^2 + \left(\frac{d}{2}\right)^2}}\right] \cdot n - F_j}{\mu} \tag{4}$$

Where S is the length of the whole plant center to the bottom (mm). And d is the plant diameter of the whole bunch of plants (mm).

By derivation, it can be obtained that when the comb structure is combing and scraping berries. The clamping force required at the upper clamping place is not only related to the fruit-stalk bonding force and the fruit-stalk-stem bonding force of the plant itself, but also to the plant diameter and plant height.

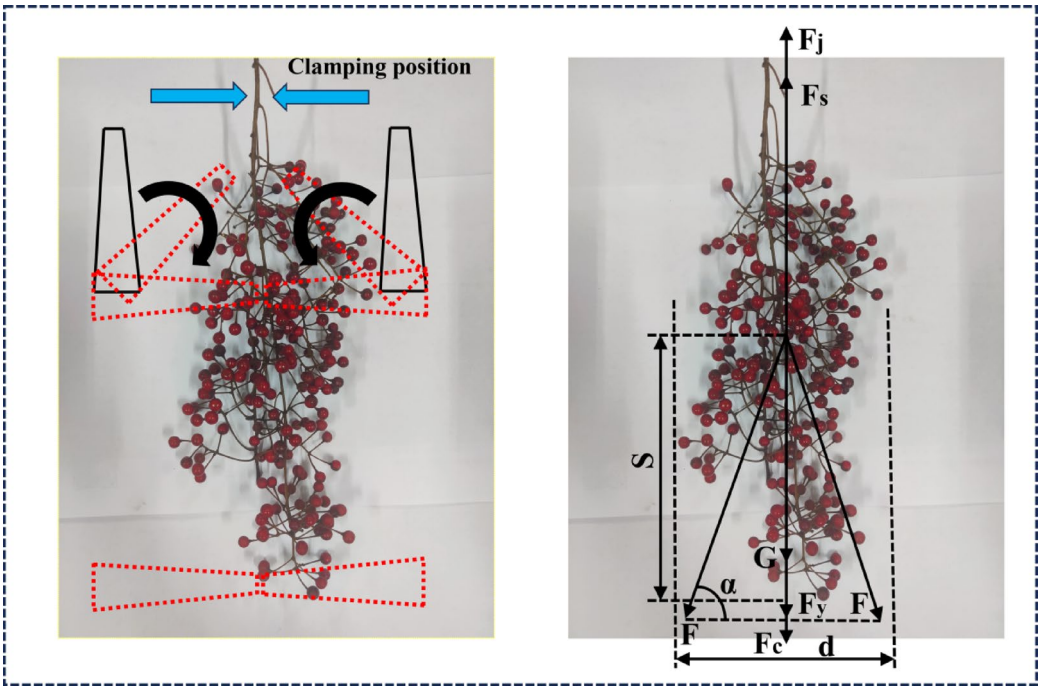

Fig. 4. Whole cluster force analysis.

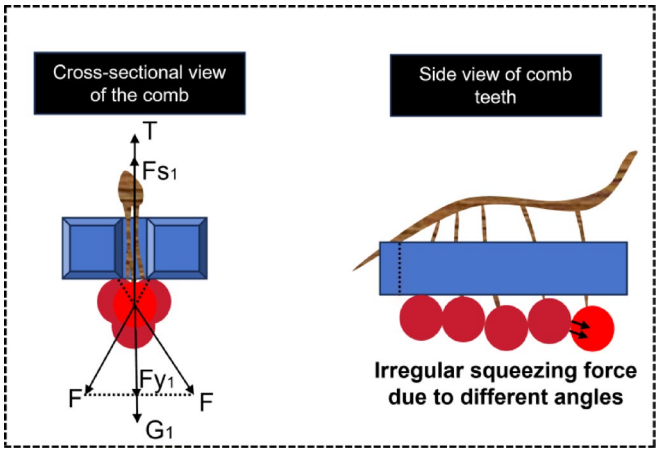

Fig. 5. Force and morphology under single-particle combing conditions.

Name	Parameters
Overall size (L×W×H)/ (mm)	325×240×370
Comb plate size/ (mm)	225×90×15
Clearance of the comb teeth/ (mm)	3
Geared motor (comb scraper)/ ($r \cdot min^{-1}$)	MGL42GP-775/0-100
Geared motor (clamping)/ ($r \cdot min^{-1}$)	5840-31ZY/0-160

Table 3. Parameters of the whole machine of Yamagata seed threshing and picking machine.

Furthermore, it is necessary to analyze the force exerted on a single berry during the actual harvesting process, As shown in Fig. 5. So as to determine the range of downward force on the comb plate. In order to ensure that the fruit is separated from the stalk and the stalk does not fall off from the main stem, the following conditions must be met:

$$F_{s1} + T \geq G_1 + 2F_{y1} \geq T_1 \tag{5}$$

where Fs1 is the friction (N) between the fruit stalk and the toothed comb gap. However, due to the small contact area, the pressure between the stems and their gaps varies depending on the growth of the shoots and the location of the harvesting device. Therefore, it cannot be calculated precisely. Therefore, it is calculated according to half of the fruit-stem binding force. T is the adhesion of peduncle-apotopic (N). G_1 is the weight of the berry (N). Fy1 is the downward squeezing force (N) of the two teeth on the berry. T_1 is the fruit-stem binding force (N).

The downward pressure required for a single berry can be obtained by bringing the data from Table 2 for large fruit binding force into Eq. (5):

$$10.8375N \geq F_{y1} \geq 3.2735N \tag{6}$$

During the threshing process, the number of particles contacted by all gaps of the combing plate each time is distributed between 20 and 30 particles. Take 25 particles for substitution. At the same time, considering that compression and collision between berries will occur during the threshing process, a safety factor of 1.3 is introduced on this basis. Therefore, the down pressure range of a single combing plate is obtained:

$$173.109375N \geq F_{y1} \geq 53.194375N \tag{7}$$

Structure and working principle of the whole machine

The whole device mainly includes the clamping device (trapezoidal screw, gear motor, serrated clamping plate), the picking inner cavity (toothed comb plate, guide rail, frame), and the power transmission device (coupling, gear motor, motor forward and reverse speed control device), etc. The parameters of the device are shown in Table 3; the overall structure of the whole machine is shown in Fig. 6.

The whole machine uses four comb plates, which are installed in two layers, with the aim of shortening the movement stroke and improving the recovery efficiency. There is a transmission gear at the journal of each comb plate, and the upper and lower rows of carding plates are synchronously turned through the rack under the control of the motor. It is then locked by means of a limit lock. Finally, the external motor drives the inner cavity downward through the synchronous belt, so as to realize the threshing of the fruit.

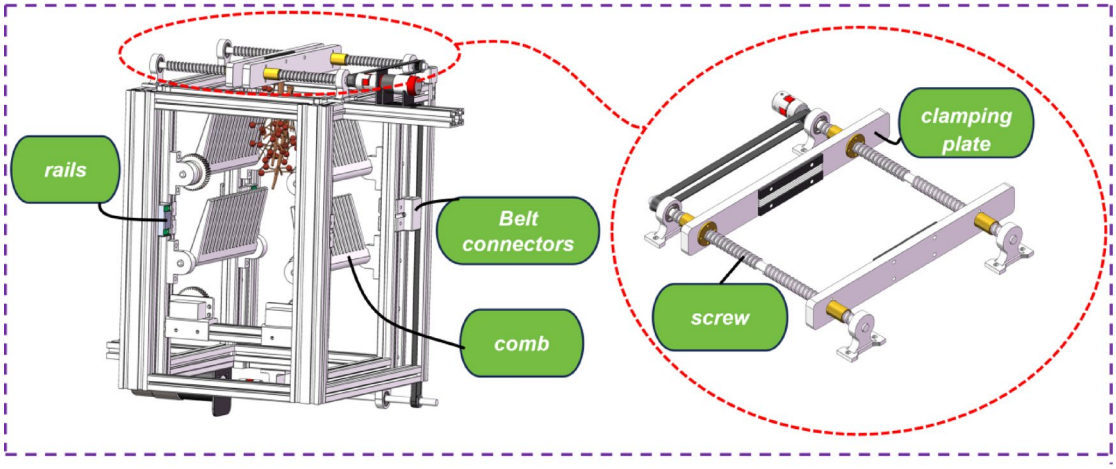

Fig. 6. The structure of the whole machine of the Idesia Polycarpa Maxim picking machine.

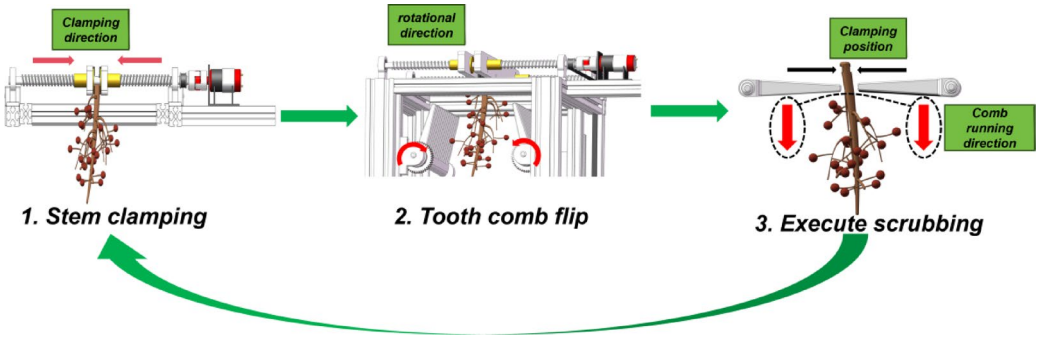

Fig. 7. The working principle and process of the picking mechanism.

When the fruit enters the interior of the device, the motor fixed on the external beam transmits the motion to the screw connected to it through a coupling. At this time, the double-acting nut on the screw will drive the clamping component to perform an opening and closing motion. This ensures the clamping and release actions on the upper end of the main stem.

Furthermore, two motors fixed on the cross beam of the inner cylinder by brackets have an active gear at each extending end. The gears mesh with the racks on both sides equipped with guides, and then the power is transmitted to the driven gears fixed on the comb plate. This achieves the synchronous flipping of the two rows of comb teeth. When the comb plate flips to a horizontal state, it enters the combing operation process. The overall operation process and working condition illustration are shown in Fig. 7.

Device component simulation and emulation

The model of the whole machine was modeled using Solidworks software[36] and assembled. And when the model was established, in order to achieve docking with ANSYS software[37].

During the whole working process, the four comb plates of the whole device all play the role of scraping. However, the two combs below are subjected to the most force. The two upper combs are designed to shorten the stroke and to clean up the remaining particles. Therefore, the working conditions of the two comb plates below are mainly analyzed.

Specifically, the comb plate is imported into the transient analysis module for analysis. Due to the irregular cluster of berries in the form of irregular grape-like bunches. Therefore, in order to simulate the effect of the center of the comb plate being affected by the reaction force of the mountain tree during the actual picking process. The Design Modeler interface in ANSYS Workbench divides the surface of the toothed comb into semicircular areas; The overall comb plate is still divided and improved by the automatic method. The upper part of the semicircle is divided by tetrahedral meshing, the element size is 1.5 mm, and the algorithm adopts the patch conformal method. The required materials are as shown in Table 4.

Working condition application: add slewing pairs to the journals and bearing supports at both ends of the comb plate. At the same time, a rotational speed is applied so that the comb plate can move from the vertical state to the horizontal working state. During this process, the comb plate touches the top fruit of the entire cluster, which can be seen as a surge of force. In the intermediate working phase, the number of berries is gradually maintained in a certain quantity, which can be considered as the maintenance of force. In the final stage, the

Name	Density	Young's Modulus/MPa	Poisson's Ratio	Shear Modulus/MPa
Steel	7.85e-006	2.e+005	0.3	76,923
ABS	1.03e-006	1628	0.4089	577.76

Table 4. Simulation material parameters.

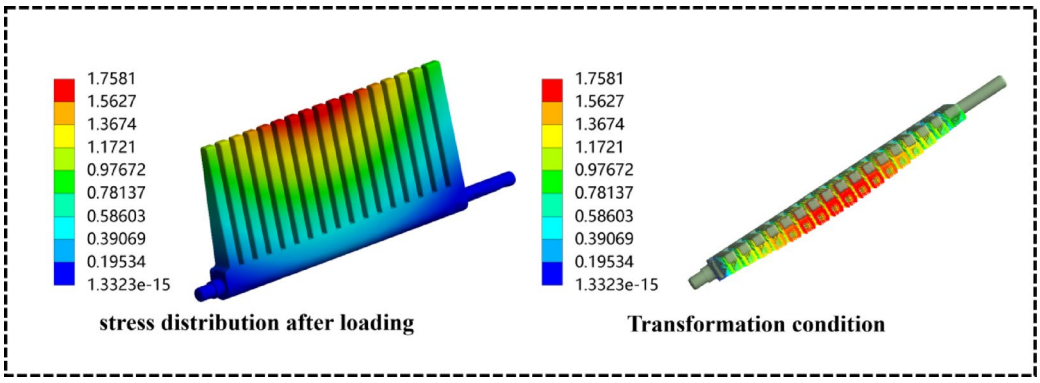

Fig. 8. Finite element analysis of comb plates.

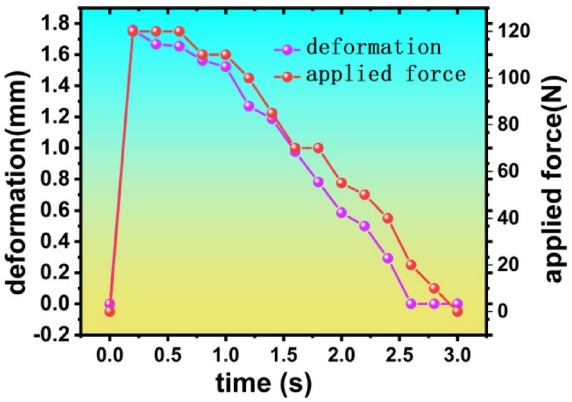

Fig. 9. The applied force and the deformation curve of the comb plate.

number of berries decreases significantly, at which point there is a subsidence of the force. Therefore, it is applied with a variable force that conforms to this law. In this case, check the deformation of the comb plate. This is shown in Fig. 8. The results of the variable force application and the deformation curve are shown in Fig. 9.

The simulation time is determined based on the time required for the actual work:

The motor speed for controlling the up and down operation of the comb plate is $n = 100$r/min; the diameter of the drive pulley is d = 15 mm; the stroke is L = 240 mm, so it can be obtained as follows:

$$v = \frac{n\pi d}{60} = \frac{100 \cdot \pi \cdot 0.015}{60} = 0.0785 \tag{8}$$

$$t = \frac{L}{v} = \frac{0.24}{0.0785} = 3.057s \tag{9}$$

From the calculation, it can be obtained that it takes 3.057s for the comb scraping action of the comb plate to be carried out downward. However, the time when the comb plate runs for the whole stroke. According to the data in Table 2, the height of the whole cluster is below 200 mm. Therefore, the operation of the comb plate after this can be regarded as not being subjected to force, therefore, the simulation time is taken as 3s for the simulation.

From the Fig. 8, it can be seen that in the comb plate into the comb scraping process of a moment. Due to the comb plate contact to the Idesia Polycarpa Maxim seed, by its resistance surge, the comb plate produced a maximum of 1.7581 mm deformation. In the force to maintain the stage of the deformation of the comb plate is gradually reduced, until to the force of the abatement of the stage of the comb plate to return to the original state.

The comb plate is 3D printed and manufactured with ABS material. which is an engineering plastic with excellent performance and widely used in the existing industrial field. The tensile strength of the pure ABS printed specimen is up to 42.9MPa[38,39]. The results show that there are large stress concentrations in the journals

at both ends of the comb plate, the maximum is up to 36.563 MPa, which is smaller than the tensile strength of the printed material. The result shows that there is a large stress concentration at both ends of the journal of the comb plate, the maximum is 36.563 MPa, which is less than the tensile strength of the material printout.

Meanwhile, for the comb plate in the execution of comb scraping action of the stress situation analysis is shown in Fig. 10. Similarly, when the combing and scraping action is performed, the equivalent force between two neighboring teeth at the root of the teeth is high. But within the permissible range of the material.

Simulation of harvest dynamics

Due to the complex and difficult-to-monitor dehulling process of the Idesia Polycarpa Maxim, a whole cluster of tung oil seed model is established in Adams[40] using flexible links[41]. The establishment of flexible bodies can be divided into discrete and modal types. Discrete flexible bodies are formed by constructing multiple small units that can be set to a certain number, and these units are connected by flexible beams. This simulates the deformation state of the flexible body after it is subjected to force, and the model still belongs to the rigid body category in essence. This method of flexible body construction is simple and has high solution efficiency, suitable for solving general deformation body problems and qualitative analysis. Modal flexible bodies are generated by finite element software and can perform mesh modeling according to the actual structure of the object[42]. Since modal linear superposition is used to simulate the deformation of the object, modal flexible bodies are only suitable for linear structural force analysis.

The method of monitoring the fall of berries can be realized by using a combination of sensors and script simulation. That is, the sensor monitors the predetermined value, and after meeting the conditions, the failure of the connection relationship is realized according to the predetermined script. However, this method is only suitable for relatively simple fall situations, and it is difficult to monitor complex multiple situations. Therefore, a generalized force combined with sensors is used to control and realize the separation of the fruit stalk and the berry[43]. The generalized force consists of three components of force and three torques, which is the interaction force between the berry and the fruit stalk. At the same time, sensors are used to monitor this generalized force. When the generalized force exceeds the predetermined bonding force, that is, the generalized force between the berry and the fruit stalk becomes 0, the berry and the fruit stalk will separate. The technical route is shown in Fig. 10. Taking the stiffness K of the connection between the seedling berry and the fruit stalk as 400 N/m, and the damping coefficient C as the default value, the component of force in the x-direction can be expressed as:

F(x) = -(400 + IF(SENVAL(SENSOR_1):0,0,-400))*DX(MARKER_567,MARKER_568,MARKER_568)-(0.1 + IF(SENVAL(SENSOR_1):0,0,-0.1))*VX(MARKER_567,MARKER_568,MARKER_568).

Where SENSOR_1 is the sensor that monitors the distance between the two action points; IF() is the judgment function; SENVAL() is the time used to read the sensor triggered; MARKER_567 is the action point located in the berry; MARKER_568 is the action point located in the stalk, generalized force the rest of the components of the force and so on, and the workflow is shown in Fig. 11.

According to the measured data related to the mountain tung tree. The air-dry density, full-dry density and basic density of Sambucus wood are 0.456 g/cm^3, 0.404 g/cm^3, 0.384 g/cm^3 [44].The overall size parameters of the flexible body are assigned: the overall height is set to 100 mm, and the diameter of the main branch is set to 4 mm; The diameter of the fruit stalk is set to 1 mm; The diameter range of berries is set between 6 ~ 10 mm, and the relevant setting parameters of fruit branches and berries are shown in Table 5.

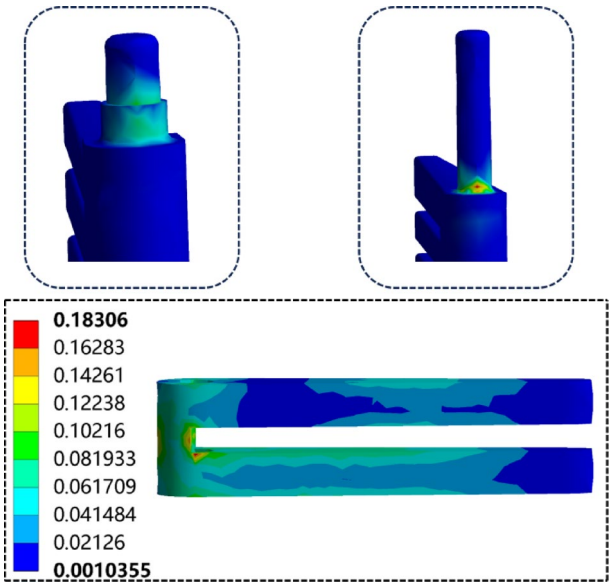

Fig. 10. The elastic strain strength of the adjacent two teeth.

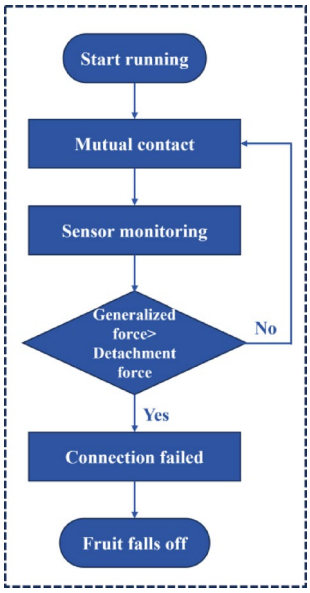

Fig. 11. Simulation technical route.

Name	Density (Kg/m^3)	Poisson's Ratio	Elastic modulus (MPa)
Berry	1119	0.32	20.5
Fruit stalk	404	0.33	3900

Table 5. Simulation parameters.

The rest of the conditions were imposed: the contact force was added between the comb plate and the fruit stalk, fruit branch and berry, the contact force was added between the fruit stalk and the fruit branch, the fruit stalk and the berry, and the collision type was solid to solid, K was taken to be 1×10^5N/m, and C was taken to be the default value. The upper end of the whole cluster flexible body model is fixed on the ground at the position of the main peduncle, and the comb plate is fixed on the ground by the translating vice, and is driven by the motion on it, and the comb plate moves downward along the direction of gravity to realize the combing action. The process and results are shown in Fig. 12.

Due to the comb scraping and threshing process comb plate will collide with flexible fruit branches, berries, etc., it is very easy to produce a more high-frequency response[45]. At the same time, it will cause the failure of the integral solver. So, in order to avoid the failure of the solution and improve the success rate, using a single comb plate and set up a good connection relationship with the above conditions imposed. Simulation of the various parameters are set as follows: the simulation time is 5s, the number of steps is set to 300 steps, the integral format for the SI2, under this integral format, the pathology of Jacobian matrix can be avoided, and the constraint equations are considered, and the solution time is longer but the accuracy of the solution is high.

In order to determine whether the different tooth shapes of the comb plate will produce different effects in the end when the berries are scraped off by the comb. The comb plate with rectangular, rhombic and circular cross sections was introduced under the same mechanical environment and driving conditions. And in the comb scraping process, the maximum separating force that can be achieved by the comb scraping of a single berry was detected respectively. And the results showed that: the maximum separating force generated by the comb plate with rectangular cross section was 7.5 N, the maximum separating force generated by the comb plate with rhombic cross section was 15 N, and the maximum separating force generated by the comb plate with circular cross section was only 2.1 N. At the same time, by comparing the three kinds of comb plate in the comb scraping work for the berries to produce the speed of the oscillation as well as the time used by the berries to be threshed. The results show that: the rectangular plate produces a more intense speed oscillations, the circular comb plate is second to the smoothest that is the rhombus comb plate. While comparing the three kinds of different tooth shape in the comb scraping work for a single berry to achieve the largest separation force. At the same time, comparing the working time of the three comb plates with different tooth shapes, the time of berry threshing is almost the same. As shown in Fig. 13. Therefore, it can be considered that the comb plate with rhombic cross-section is more suitable for the demand.

Experimental section

To verify the different effects produced when using different cross-sectional shapes of comb teeth during the simulation test. The same material is used to obtain three comb teeth plates with different cross-sectional shapes:

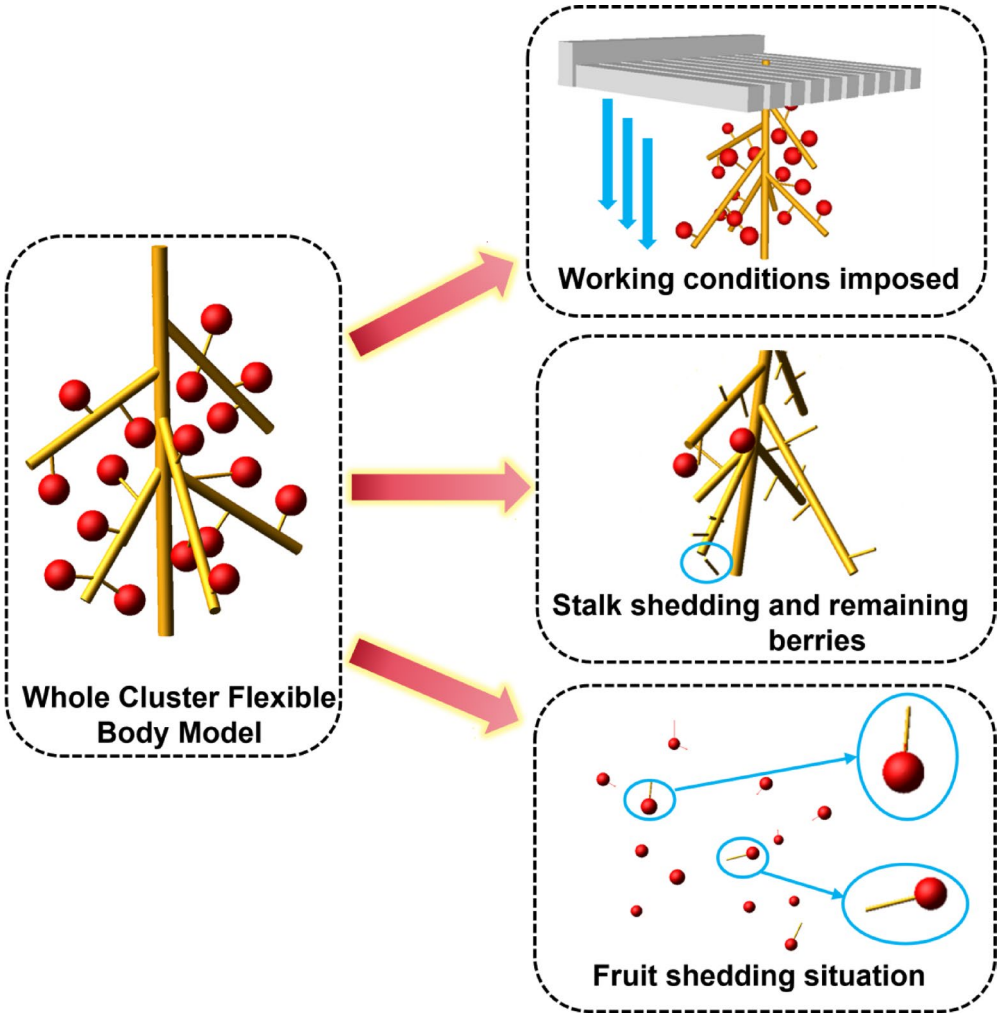

Fig. 12. Cluster flexible linkage model.

rectangular, rhombic, and circular. As shown in Fig. 14. The experimental materials are from the mountain ash planted in the Forestry School of Guizhou Province. The experiment is carried out by controlling variables and combining the measured berry size to specify that the gap between the teeth of the three comb tooth plates is 4 mm. While ensuring the same running speed during the movement; and select fruits with similar chains for testing: that is, control the number of berries manually to be the same. And finally, based on this, perform five single-factor bench tests with cross-sectional shape as the single factor. And take the mean value as the indicator, the overall experimental scene and equipment layout are shown in Fig. 15.

Through the experiment. We can obtain the effect of the selected tooth cross-section shape on the performance indexes such as picking rate, breakage rate and impurity rate under the control of the rest of the variables. Specifically, the picking rate is 80.54% and the stalking rate is 75.77% when the comb cross-section is rhombic. Which is 8.06% and 3.47% higher than that of the comb with rectangular cross-section. And 10.38% and 12.06% higher than that of the comb with rounded cross-section. The increase was 10.38% and 12.06% respectively, so it can be considered that the comb with rhombic cross-section is the best. See Table 6 for details.

In order to further explore on the basis of some factors on the desired characterization of performance indicators. Combined with the harvesting method and the movement mode, selected comb tooth gap and comb plate overall running speed as factors for the test, the specific experimental results are shown in Fig. 16.

On the basis of single-factor test, further explore the effect of the interaction of comb gap and comb running speed on the performance indexes, so that the optimal inter-tooth gap and running speed can be determined. Therefore, through the central composite design CCD (central composite design) response surface test method on the comb gap, comb running speed test, the number of tests for 13 times, including the center of the point at the 5 groups of repetitive experiments, the experimental factor level coding table is shown in Table 7. The experimental design arrangements and the results are shown in Table 8.

$$Y_1 = 7.00034 + 21.05082X_1 + 783.83190X_2 + 23.25000X_1X_2 - 2.28308X_1^2 - 9068.31897X_2^2$$

$$Y_2 = -3.43759 + 1.80032\,X_1 + 95.86494X_2 + 29.25000X_1X_2 - 0.324698X_1^2 - 2546.98276X_2^2$$

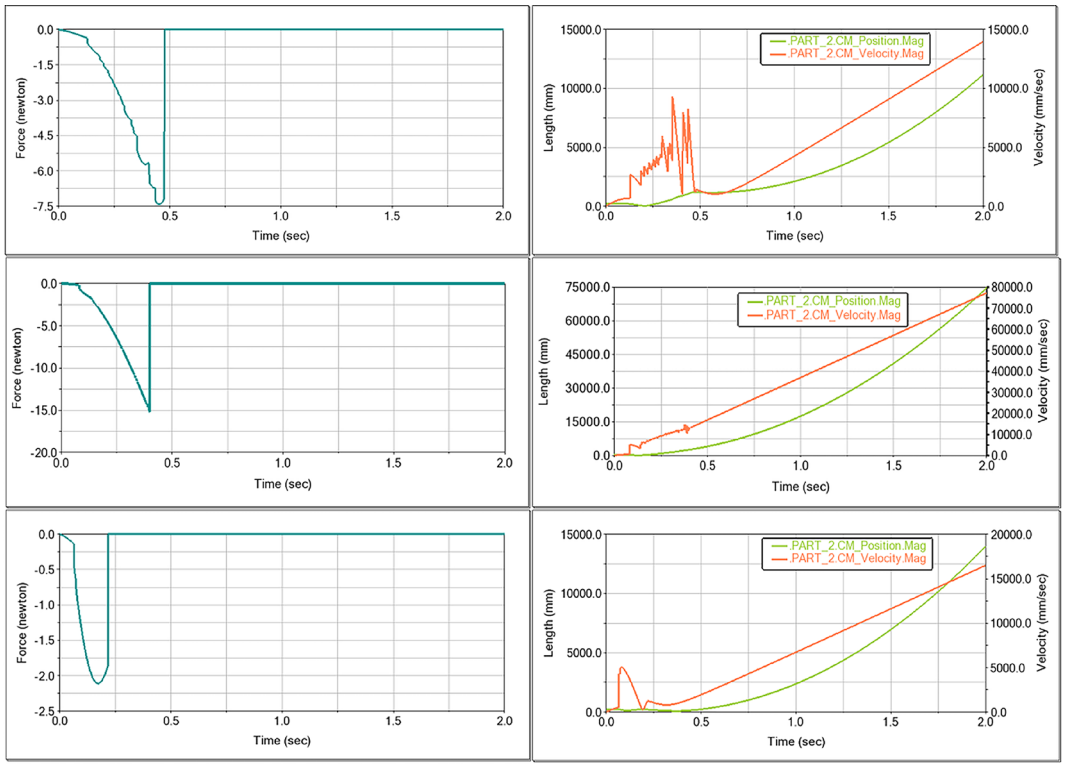

Fig. 13. Cluster flexible linkage model.Note: From top to bottom are comb plates with rectangular, diamond and round cross sections, Comparison of binding force on the left; berry shedding time and rate curves on the right.

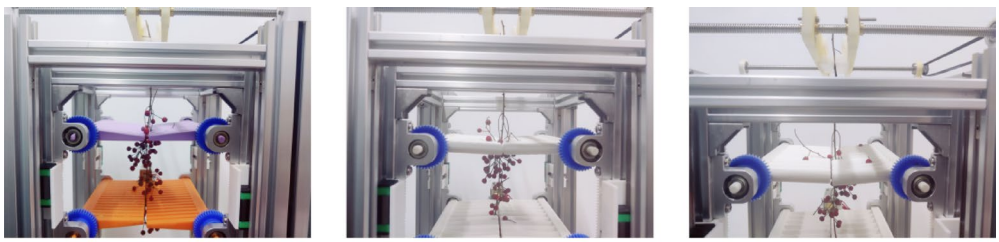

Fig. 14. Different shapes of comb teeth comb plate layout.

$$Y_3 = -91.11023 + 35.12904X_1 + 3055.98707X_2 - 131.50000X_1X_2 - 2.82274X_1^2 - 23689.87069X_2^2$$

The ANOVA of the regression equations of Y_1, Y_2 and Y_3 are shown in Table 9 which showed that the regression model P of the picking rate Y_1 was 0.0387. The regression model P of the breakage rate Y_2 was 0.0174, and the regression model P of the Stemming rate Y_3 was 0.0027. Which indicated that the regression model was significant, and the coefficients of determination, R^2, were 0.7599, 0.8128, and 0.8935. Respectively, which were all close to 1, indicating a good fit of the regression equation.

Results and discussion

As can be seen from Table 9. The comb clearance has a significant effect on the picking rate. While the traveling speed has a non-significant effect on it. On the contrary, the traveling speed has a significant effect on the breakage rate. For the infarction rate, the comb clearance and the traveling speed have a non-significant effect on it, and on the whole, the effect of the comb clearance is greater than the traveling speed. Thus, the comb clearance should be the main optimization target. So as to increase the picking rate and the Stemming rate, and further reduce the Breakage rate. Based on the fitting equation of Y_1, Y_2, Y_3, using origin software for the response surface graphics as well as the contour graphics as shown in Fig. 17.

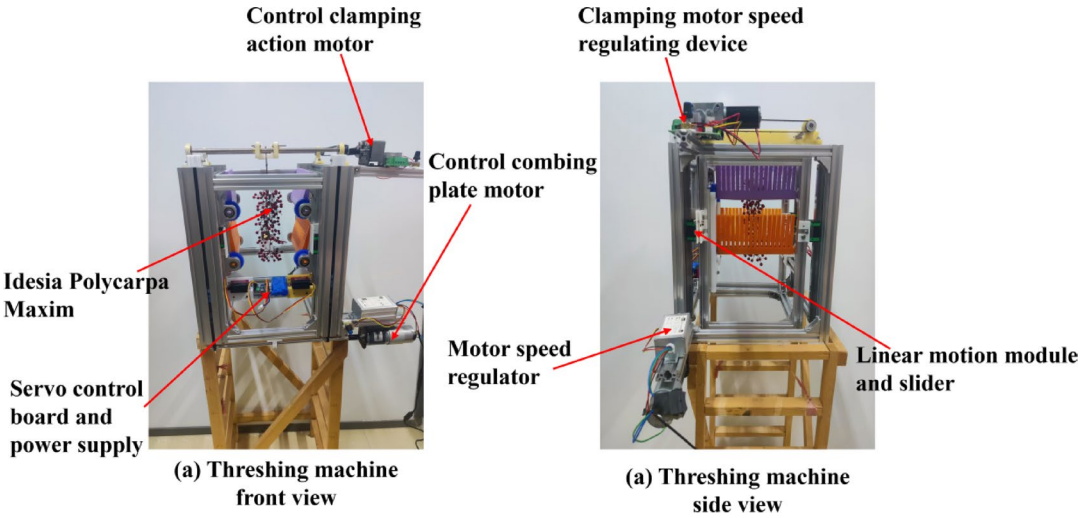

Fig. 15. Experimental equipment and layout.

Section shape	picking rate/%	Breakage rate/%	Stemming rate/%
rectangles	72.48	3.38	72.30
rhombic	80.54	3.24	75.77
orbicular	70.16	2.41	63.71

Table 6. Impact of different comb cross-sectional shapes on harvesting.

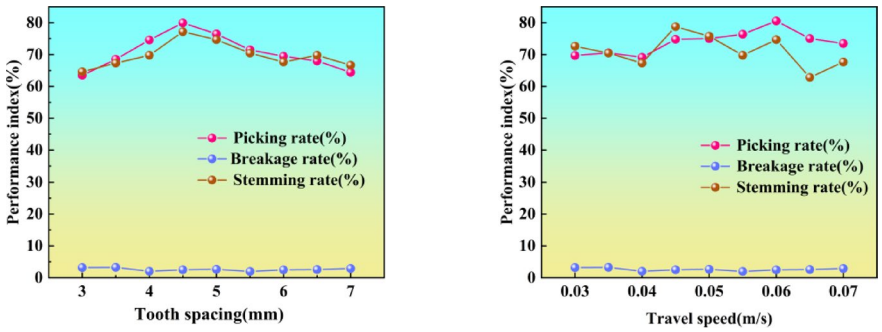

Fig. 16. Influence of comb gap and travel speed on performance indicators.

Influence of comb gap and travel speed on performance indicators Level	Factors	
	Comb tooth gap X_1/(mm)	Movement speed X_2/(m/s)
-2	3	0.03
-1	4	0.04
0	5	0.05
1	6	0.06
2	7	0.07

Table 7. Experimental factor level coding table.

In order to further obtain the parameters of the optimal operation of the threshing device. The three regression models were optimized using the Numerical module of the Design-Expert software, and the optimization constraints were determined based on the actual operational requirements and the results of the model analysis:f the model analysis:

No.	Factor		Performance indexes		
	Tooth spacing X_1/(mm)	Movement speed X_2/(m/s)	Picking rate Y_1/%	Breakage rate Y_2/%	Stemming rate Y_3/%
1	5	0.05	77.78	3.17	72.63
2	6	0.04	70.55	2.03	70.45
3	6	0.06	70.83	2.48	67.31
4	5	0.05	77.99	3.68	78.78
5	5	0.05	80.54	3.24	75.77
6	7	0.05	69.12	2.12	64.61
7	5	0.05	76.38	3.18	74.69
8	5	0.07	74.81	2.02	66.67
9	5	0.05	79.01	3.31	72.82
10	4	0.06	73.48	1.94	69.77
11	5	0.03	75.03	2.64	64.39
12	3	0.05	69.71	1.98	62.82
13	4	0.04	74.13	2.66	67.65

Table 8. Experimental design and results. Response surface regression analysis was performed by Design-Expert 13.0 software to analyze the results of comb gap and running speed. And the fitting equations of each influencing factor with the evaluation indexes Y_1, Y_2, and Y_3 were obtained after relevant calculations as follows:

Source	Picking rate (%)		Breakage rate (%)		Stemming rate (%)	
	F-value	*P*-value	F-value	*P*-value	F-value	*P*-value
Mode	4.43	0.0387*	6.08	0.0174*	11.74	0.0027**
X_1	0.8047	0.3995	0.0253	0.8780	0.2971	0.6026
X_2	0.0096	0.9246	1.60	0.2463	0.2423	0.6376
$X_1 \times_2$	0.0380	0.8509	2.88	0.1334	1.60	0.2457
X_1^2	21.00	0.0025**	20.35	0.0028**	42.36	0.0003**
X_2^2	3.31	0.1115	12.52	0.0095**	29.84	0.0009**
Lack of fit	4.21	0.0992	4.89	0.0797	0.2550	0.8547

Table 9. Regression equation analysis of variance. Note: * indicates a significant correlation ($0.01 < P \leq 0.05$), ** indicates an extremely significant correlation ($P \leq 0.01$).

$$\begin{cases} \mathbf{max} \boldsymbol{Y}_1 (\boldsymbol{X}_1, \boldsymbol{X}_2) \\ \mathbf{min} \boldsymbol{Y}_2 (\boldsymbol{X}_1, \boldsymbol{X}_2) \\ \mathbf{max} \boldsymbol{Y}_3 (\boldsymbol{X}_1, \boldsymbol{X}_2) \\ s.t. \begin{cases} 3 < \boldsymbol{X}_1 \leq 7 \\ 0.03 < \boldsymbol{X}_2 \leq 0.07 \end{cases} \end{cases} \tag{10}$$

Verification experiment

Optimized solution for the optimal parameter combination: When the comb gap is 4.40709 mm and the travel speed is 0.05999 m/s, the picking rate is 75.961%, the Stemming rate is 72.19%, and the breakage rate is 2.51%. The optimized results are rounded, setting the comb gap to 4.5 mm and keeping the travel speed constant at 0.06 m/s. Under these conditions, 5 repeated experiments were conducted. The test results show that the mean values of the optimized performance parameters are 8.01%, 34.33%, and 5.41% higher than the mean values before optimization, as shown in Table 10. If the breakage rate is used as an indicator for comparison, the device still has a high degree of applicability[46–50].

Conclusions

Idesia Polycarpa Maxim is widely distributed in high altitude slopes, valleys and other places, and it is difficult for larger harvesting machinery to carry out work due to terrain restrictions. As a result, harvesting can usually only be done manually by cutting the entire cluster. However, the subsequent processing still requires manual removal of the berries. Not only is it time-consuming, but it can also easily lead to berry damage. Eventually, it will accelerate the rate of oxidative deterioration of the fruit. Therefore, in order to solve the problem of mechanized picking and threshing of Idesia Polycarpa Maxim, this paper designed a small equipment with integrated picking and threshing, which is suitable for various terrains such as mountainous areas. In this paper, the device is simulated by finite element analysis, and the experimental experiments are designed based on

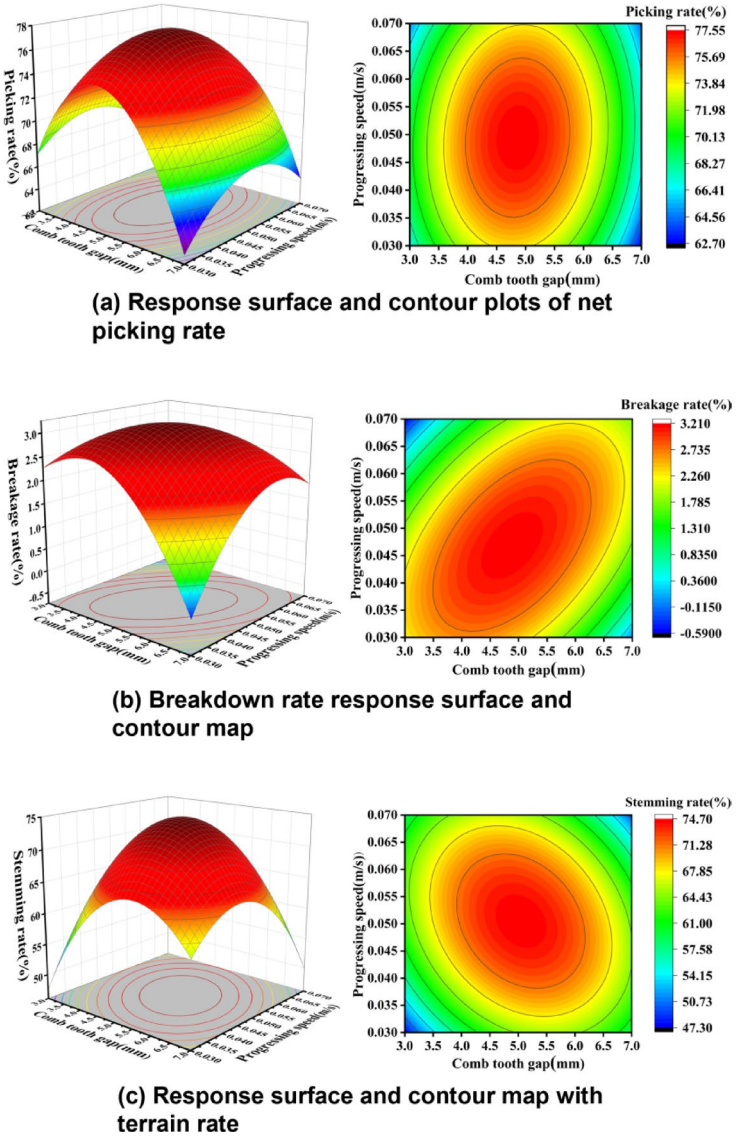

Fig. 17. Response surfaces and contour plots for each performance indicator.

Test number	Picking rate/%	Breakage rate/%	Stemming rate/%
1	81.1	1.52	72.46
2	79.55	2.01	73.67
3	83.66	1.41	74.97
4	80.67	1.84	73.5
5	77.78	1.9	73.65
Average value	80.55	1.74	73.65

Table 10. Test results after optimization of parameters.

the simulation results, and the optimal parameters of the key components of the device are obtained. After the verification experiment was carried out with the optimized parameters, all performance indicators were improved. Finally, a kind of integrated small mechanical equipment for picking and threshing of Idesia Polycarpa Maxim was developed.

1. The physical and mechanical properties of the Idesia Polycarpa Maxim indicate that the bonding force range between the fruit and the fruit stalk is: 4.5 ~ 7.98 N. The bonding force range between the fruit stalk and the fruit peduncle is: 0.63 ~ 4.33 N. The size parameters show that the particle size mean is 7.36 mm. Based on this,

a picking and threshing integrated device based on the comb-tooth type was designed. Theoretical derivation shows that the power range of the comb-tooth structure in removing the berry is 53.194 $N \sim 173.109$ N.

2. Finite element analysis was conducted on the comb plate section. The maximum deformation of the component under the action of the given variable force is 1.7581 mm. The maximum stress load on the comb teeth during the working process is 36.563Mpa, which is also within its allowable range. Furthermore, a dynamic simulation of the picking process was carried out. Under this process, the diamond-shaped cross-section comb teeth were determined to be the best tooth shape for the equipment. Under this tooth shape, the maximum separation force generated on the berry reaches 15 N, which is higher than the 7.5 N of the rectangular comb teeth and the 2.1 N of the circular comb teeth. At the same time, the vibration and surge generated by the entire working process under the diamond comb teeth are the best.
3. After determining through a single-factor experiment that the diamond cross-section comb teeth are indeed superior to other tooth shapes, further parameter optimization is carried out. The Picking rate, breakage rate, and Stemming rate are selected as performance indicators, and bench tests are conducted with comb tooth gap and travel speed as factors. A response surface analysis based on the central composite design is also performed, showing that the performance indicators are at their best when the comb tooth gap is 4.5 mm and the travel speed is 0.06 m/s. Verification experiments using the optimized parameters show that the Picking rate, breakage rate, and Stemming rate are increased by 8.01%, 34.33%, and 5.41% respectively. This result further indicates that the device designed in this paper can effectively carry out mechanized harvesting of the Idesia Polycarpa Maxim.

This study fills the gap in the mechanized harvesting of Idesia Polycarpa Maxim. The designed integrated picking and threshing equipment is more suitable for mountainous terrain. It can not only reduce labor input but also improve the efficiency of threshing. This study can provide a reference for the design and improvement of harvesting equipment for clustered crops. In this study, only a specific variety produced in Guizhou was tested in the experimental stage. However, there may be certain differences in the physical properties of different varieties. In the next stage, it is still necessary to verify the applicability of the equipment for different varieties. In the future, the equipment can be automated for harvesting by pairing with mobile platforms and collection devices, while combining visual recognition to further increase its degree of automation.

Data availability

Data cannot be shared openly but are available on request from correspondence author.

Received: 28 February 2025; Accepted: 9 June 2025
Published online: 30 September 2025

References

1. Lingli, W. U. et al. Research progress in the development and utilization of idesia polycarpa. *Non-wood For. Res.* **41**, 242–252. https://doi.org/10.14067/j.cnki.1003-8981.2023.02.025(2023) (2023).
2. Guofu, D. A. I., Shiyou, X. I. E. & Teng, W. A. N. G. AN Xiaofeng. Idesia polycarpa's characteristic,value in use and cultivation techniques. *Hubei Agri. Sci.* **50** 08 1615–1618.https://doi.org/10.14088/j.cnki.issn0439-8114.2011.08.060(2011).
3. Xie Huandong et al. Changes in oil accumulation and nutritional component contents during Idesia polycarpa fruit development. *Non-wood Forest Res.* 1–10. (2024). http://kns.cnki.net/kcms/detail/43.1117.S.20240926.1451.004.html
4. Wang et al. A flowering morphological investigation, fruit fatty acids, and mineral elements dynamic changes of Idesia polycarpa Maxim. *Plants* **13** 18 2663 (2024).
5. Li et al. An investigation of the growth status of 19-year-old idesia polycarpa 'yuji'plantation forest in the mountainous region of Henan. *China Heliyon*. **9**, 9 (2023).
6. Zhang et al. Analysis of chemical composition and antioxidant activity of idesia polycarpa pulp oil from five regions in China. *Foods* **12** 6 1251 (2023).
7. Guo et al. A systematic study on composition and antioxidant of 15 varieties of wild idesia polycarpa fruits in China. *Front. Sustainable Food Syst.* **7**, 1292746 (2023).
8. Fang et al. Influence of fruit color on the oil quality and seed germination of idesia polycarpa Maxim. *J. Seed Sci.* **45**, e202345033 (2023).
9. Li et al. Investigation and analysis of the current status of wild Chinese idesia Polycarpa Maxim resources in Guizhou area. *Agric. Technol.* **44.16**, 62–66. https://doi.org/10.19754/j.nyyjs.20240830014 (2024).
10. Menghuan, Z. H. A. O. et al. Analysis of fruit quality of Idesia polycarpa Maxim at different harvest periods. *Journal of Henan Agricultural University* 58.01:69–77. (2024). https://doi.org/10.16445/j.cnki.1000-2340.20231213.001(2023).
11. LIU et al. Study on the optimization of response surface of different pretreatment methods to the preparation of Idesia polycarpa oil by cold pressing method. *J. Henan Agri. Univ.* 1–20. https://doi.org/10.16445/j.cnki.1000-2340.20240429.006(2024).
12. Feida, D. I. et al. Effect on drying characteristics and oil quality of idesia polycarpa maxim.var.vestita diels treated by different sample layers of hot air drying. *Farm Prod. Processing* **24**11–16 https://doi.org/10.16693/j.cnki.1671-9646(X).2018.12.038(2018).
13. Wang, J. Effects of Different Processing Techniques on the Quality of Idesia Polycarpa Oil.2017. *Henan Agricultural University*, MA thesis. (2017). https://doi.org/10.27117/d.cnki.ghenu.2017.000165
14. Zhang et al. Transcriptome analysis reveals the role of temperature in seed germination of idesia polycarpa Maxim through the integration of phytohormones and sugar metabolism. *Brazilian J. Bot.* **47.4**, 963–979 (2024).
15. Rana, S. et al. Study of the pattern of reproductive allocation and fruit development in young dioecious trees of idesia polycarpa Maxim. *South. Afr. J. Bot.* **146**, 472–480 (2022).
16. Li et al. Transcriptome analysis of idesia polycarpa maxim. Var vestita diels flowers during sex differentiation. *J. Forestry Res.* **31**, 2463–2478 (2020).
17. Kwon, C. S. et al. Anti-leukemic effects of idesia polycarpa Maxim branch on human B-cell acute lymphoblastic leukemia cells. *Curr. Issues. Mol. Biol.* **45.5**, 4035–4049 (2023).
18. Huang et al. Polyphenolic compounds from idesia polycarpa maxim. Fruits ameliorate non-alcoholic fatty liver disease by modulating lipid metabolism in oleic acid-induced HepG2 cells and high-fat diet-induced mice. *J. Funct. Foods.* **108**, 105715 (2023).
19. Lee, M. et al. Anti-adipogenic activity of compounds isolated from idesia polycarpa on 3T3-L1 cells. Bioorganic & medicinal chemistry letters 23.**11** 3170–3174 (2013).

20. Chen, B. et al. Design and optimization of a negative pressure rotary cutting safflower filaments harvesting device. *Sci. Rep.* **15**1 9693 (2025).
21. Zhu, H. et al. Design and experimental study on pruning machine of Yunnan edible Rose. *Sci. Rep.* **13.1**, 4118 (2023).
22. Li, T., Guan, X. & Zhou, F. Mechanistic analysis and experimental study of a shear-type low-loss fresh corn ear-picking mechanism. *Comput. Electron. Agric.* **213**, 108191 (2023).
23. Ghonimy, M., Alharbi, A. & Mohamed, M. Ibrahim. Damping behavior of Olive trees under trunk shaking. *Sci. Rep.* **15.1**, 11615 (2025).
24. Liu, C., Xu, D. & Cao, J. Vibration response of walnuts under vibration harvesting. *Agronomy* 13.2: 461 (2023).
25. Wu et al. Optimization and test of the operating parameters of a camellia oleifera fruit picking device under the synergistic action of a vibration comb.*Engenharia Agrícola*, **44**: e20230087 (2024).
26. Chen Haixia. Design and experiment of the flexible Combing- stripping device of alfalfa seed. *J. Agri. Mechanization Res.* **4510** 159–165 https://doi.org/10.13427/j.cnki.njyi.2023.10.020(2023).
27. Fulong, X. U. et al. Design and test of comb-toothed test bed for flax capsule comb-brushing. *J. Gansu Agri. Univ.* **5603** 159–167 https://doi.org/10.13432/j.cnki.jgsau.2021.03.020(2021).
28. Da-wei, F. A. N. G. et al. Design and experimental study of the comb-type picking test bench for cerasus humilis. *J. Gansu Agri. Univ.* **5405** 212–218 https://doi.org/10.13432/j.cnki.jgsau.2019.05.026(2019).
29. Wang et al. Design and experimental study of differential speed comb type pineapple harvesting machine. *J. Agri.Mechanization Res.* **4609** 115–120 https://doi.org/10.13427/j.cnki.njyi.2024.09.010(2024).
30. Wang et al. Design and experimental research of a comb-type Buckwheat-harvesting device. *Agriculture* **13.7**, 1383 (2023).
31. Zhao et al. A comb-brushing-type green soybean pod harvesting equipment: design and experiment. *Plos One*. **18**, 11: e0293567 (2023).
32. Li et al. Design and test of a comb-brush-type honeysuckle-picking device. *Agriculture* **13** 11 2088 (2023).
33. Wang et al. Design, simulation and test of roller comb type Chrysanthemum (Dendranthema morifolium Ramat) picking machine. *Comput. Electron. Agric.* **187**, 106295 (2021).
34. Sui et al. A comb-type end-effector for inflorescence thinning of table grapes. *Comput. Electron. Agric.* **217**, 108607 (2024).
35. Huang Xiangfei;Lu Lixin. Effect of vibration on bruising and creep property of Pear fruit. *Trans. Chin. Soc. Agricultural Eng.* **24.S1**, 34–37 (2008).
36. Solidworks2023. *18/10/2023 Dassault Systemes US* (Downloads | Support | SOLIDWORKS, May 2024).
37. ANSYS Workbench 2022R1. 9/3/2022 Ansys US. May (2024). https://www.ansys.com/zh-cn
38. Qiao Wenyu et al. Research on properties of ABS filament used in 3D printing. *Eng. Plast. Application*. **44.03**, 18–23 (2016).
39. YE Xuan;TU Huajin. Research progress in ABS materials for 3D printing. *China Plast.* **33.12**, 101–108. https://doi.org/10.19491/j.issn.1001-9278.2019.12.018 (2019).
40. View, A. May 2024 Mechanical Dynamics US. (2020). https://hexagon.com/products/product-groups/computer-aided-engineering-software/adams May 2024.
41. ZHAO Xi-fang. A study on flexible body using ADAMS. *Electro-Mech. Eng.* **03** 62–64 .https://doi.org/10.19659/j.issn.1008-5300.2006.03.018(2006).
42. Wu Bing;Chen Bo. ADAMS dynamics solution algorithm comparison and analysis. *Neijiang Sci. Technol.* **32.09**, 24 (2011).
43. Li et al. Design and experiment of wine grape threshing mechanism with flexible combing striping monomer. *Trans. Chin. Soc. Agricultural Eng.* **31.06**, 290–296 (2015).
44. Xingyue, X. I. O. N. G. Zhen. Stem analysis and physical and mechanical property determination of idesia polycarpa. *Henan Sci.* **39.11**, 1828–1833 (2021).
45. Rui, L. I. et al. Simulation analysis and parameter optimization of a prickly Ash vibration picker based on ANSYS workbench and ADAMS. *Journal Southwest. University(Natural Sci. Edition)* **4312** 57–66 https://doi.org/10.13718/j.cnki.xdzk.2021.12.007(2021).
46. Abdeen, M. et al. The impact of threshing unit structure and parameters on enhancing rice threshing performance. *Sci. Rep.* **15**1, 6250 (2025).
47. Kiniulis, V. et al. Corn ear threshing performance of filler-plate-covered threshing cylinders. *Mechanics* 23.5: 714–722 (2017).
48. Shi, R. et al. Simulation of flax threshing process by different forms of threshing drums in combined harvesting. *Agronomy* **15** (1), 36 (2024).
49. Li, X. et al. Design and test of longitudinal axial flow staggered millet flexible threshing device. *Agriculture* 12.8: 1179 (2022).
50. Ma, J. et al. Research and experimentation on sparse–dense interphase curved-tooth Sorghum threshing technology. *Agriculture* **14**10, 1722 (2024).

Acknowledgements

The study was supported by the Project Fund (0624020) of Guizhou Forestry and Grassland Development Co., Ltd.

Author contributions

G.Y. Writing-Original Draft, Methodology, Software; D.W. Funding Acquisition, Supervision, Experiment; W.X. Funding Acquisition, Supervision; Y.T. Software, Validation;

Declarations

Competing interests

The authors declare no competing interests.

Additional information

Correspondence and requests for materials should be addressed to D.W.